# PERIÓDICO TCHÊ QUÍMICA ARTIGO ORIGINAL

# IMPACTO DAS FUNÇÕES *WAVELET* NO APRIMORAMENTO DA RESOLUÇÃO DE IMAGENS USANDO PREENCHIMENTO COM ZEROS DE *WAVELET*

# IMPACT OF WAVELET FUNCTIONS ON IMAGE RESOLUTION ENHANCEMENT USING WAVELET ZERO PADDING

تأثير الدوال المويجية على تحسين دقة الصورة باستخدام التعبئة الصفرية المويجية

#### Ghusoon Mohammed Tuma \*

Department of Physics, College of Science, University of Babylon, Babel, Iraq

#### Ameerah Ab. Al-Sadooni

Department of Physics, College of Science, University of Babylon, Babel, Iraq

#### **Wasnaa Witwit**

Department of Physics, College of Science, University of Babylon, Babel, Iraq

\* Corresponding author

e-mail: sci927.guson.mohammed@student.uobabylon.edu.ig

Received 12 June 2024; received in revised form 7 July, 16 August 2024; accepted 01 October 2025.

#### **RESUMO**

Introdução: O aprimoramento da resolução de imagens é crucial em diversas aplicações; inclui a utilização de várias técnicas para melhorar a clareza e o nível de detalhes de uma imagem. As técnicas baseadas em wavelets oferecem a capacidade de realizar uma análise de multirresolução da imagem, decompondo-a em sub-bandas de baixa e alta frequência. Objetivo: Esta abordagem examina como diferentes funções wavelet impactam o desempenho da técnica de Preenchimento com Zeros de Wavelet (WZP), um método fundamental baseado em wavelets para reconstrução de imagens de alta resolução (HR). Método: A investigação inclui sete funções wavelet aplicáveis à DWT e oito métodos de interpolação. O exame concentra-se no desempenho da relação sinal-ruído de pico (PSNR) e na qualidade visual das funções wavelet. O programa é escrito em Matlab, itera sobre todas as funções wavelet e métodos de interpolação, e gera uma planilha Excel dos valores PSNR. Resultados: Foram examinadas imagens padrão, de sensoriamento remoto e astronômicas. Diferenças significativas foram encontradas entre as funções wavelet e métodos de interpolação. Métodos de interpolação avançados, como bicúbico e Lanczos, alcançaram PSNR mais alto. Para conjuntos de dados astronômicos, os métodos de interpolação bilinear e triangular mostraram superioridade. Para o conjunto de dados Lina, a wavelet coif2 resultou no PSNR mais alto em todos os métodos de interpolação, variando de 25,121 para o mais próximo a 26,840 para Lanczos3. Discussão: O Preenchimento com Zeros de Wavelet (WZP) minimiza artefatos de borda ao suavizar a imagem enquanto mantém as características. A eficácia do WZP depende da escolha adequada da função wavelet e do método de interpolação. As wavelets Coif2, fk8 e Bior tiveram melhor desempenho para conjuntos de dados específicos. Conclusões: O Preenchimento com Zeros de Wavelet (WZP) minimiza artefatos de borda ao suavizar a imagem enquanto mantém as características. Sua eficácia depende da escolha adeguada da função wavelet e do método de interpolação, com coif2, fk8 e Bior tendo melhor desempenho para conjuntos de dados específicos. Recomenda-se o desenvolvimento de técnicas wavelet adaptativas e o estudo de uma gama mais ampla de conjuntos de dados para melhorias adicionais.

Palavras-chave: transformada wavelet discreta, preenchimento com zeros, aprimoramento de resolução

#### **ABSTRACT**

**Background**: Image resolution enhancement is crucial in various applications; it involves utilizing different techniques to improve an image's clarity and level of detail. Wavelet-based techniques enable the performance of a multiresolution analysis of the image by decomposing it into low- and high-frequency subbands. **Aim**: This approach investigates the impact of different wavelet functions on the performance of the Wavelet Zero-Padding (WZP) technique, a fundamental wavelet-based method for reconstructing high-resolution (HR) images. **Method:** 

The investigation employs seven wavelet functions suitable for DWT and eight interpolation methods. The examination focuses on the peak signal-to-noise ratio (PSNR) performance and visual quality of wavelet functions. The program, written in MATLAB, iterates over all wavelet functions and interpolation methods, generating an Excel sheet that contains the PSNR values. **Results**: Standard, remote sensing, and astronomical images were examined. Significant differences were found among the wavelet functions and interpolation methods. Advanced interpolation methods, such as bicubic and Lanczos, achieved higher PSNR. For astronomical datasets, bilinear and triangle interpolation methods showed superiority. For the Lina dataset, the coif2 wavelet yielded the highest PSNR across all interpolation methods, ranging from 25.121 for the nearest neighbor to 26.840 for the Lanczos3 method. **Discussion**: Wavelet Zero Padding (WZP) minimizes edge artifacts by smoothing the image while maintaining features. The effectiveness of WZP depends on choosing the proper wavelet function and interpolation method. Coif2, fk8, and Bior wavelets performed best for specific datasets. **Conclusion**: Wavelet Zero Padding (WZP) minimizes edge artifacts by smoothing the image while maintaining features. Its effectiveness depends on choosing the proper wavelet function and interpolation method; coif2, fk8, and Bior perform best for specific datasets. Developing adaptive wavelet techniques and studying a broader range of datasets are recommended for further improvement.

Keywords: discrete wavelet transform, zero padding, resolution enhancement

الخلاصة

الخلفية: يعتبر تحسين دقة الصورة أمرًا بالغ الأهمية في العديد من التطبيقات، ويتضمن استخدام تقنيات متنوعة التحسين وضوح الصورة ومستوى التفاصيل فيها. توفر التقنيات المعتمدة على المويجات القدرة على إجراء تحليل متعدد الدقة للصورة من خلال تقسيمها إلى نطاقات تردد منخفضة وعالية. الهدف: يهدف هذا البحث إلى دراسة كيفية تأثير الدوال المويجية المختلفة على أداء تقنية التعبئة الصفرية المويجية والمويجية قابلة التطبيق على التحويل المويجي المنفصل (DWT) معتمدة على المويجات لإعادة بناء صور ذات دقة عالية. الطريقة: تتضمن الدراسة سبع دوال مويجية قابلة التطبيق على التحويل المويجي المنفصل (DWT) وثماني طرق توليد المبكسلات. يركز الفحص على أداء دوال المويجات من حيث نسبة ذروة الإشارة إلى الضوضاء (PSNR) وجودة الصورة البصرية. تم كتابة البرنامج بلغة ماتلاب، حيث يقوم بتكرار جميع دوال المويجات وطرق توليد البكسلات، وينتج جدول Excel على قيم PSNR. النتائج: تم فحص صور قياسية وصور استشعار عن بعد وصور فلكية. وقد وجدت اختلافات كبيرة بين دوال المويجات وطرق توليد البسكلات. حققت طرق توليد البسكلات المتقدمة، مثل Lanczos على قيم PSNR على المنسبة للصورة الفلكية، فقد أظهرت طرق توليد البسكلات للمتقدمة مثل Lanczos على مويجة وطرق التوليد المناسبة. حيث تفوقت دوال المويجات وطرق تنعيم الصورة مع الحفاظ على ميزاتها. تعتمد فعالية تقنية WZP على اختيار الدالة المويجية وطرق التوليد المناسبتين يلعب دور رئيسي في اختيار الدالة المويجية وطرق التوليد المناسبتين يلعب دور رئيسي في القائية الطريقة، اذ ان 168 (Coif2 أظهرت اعلى أداء لمجموعة بيانات معينة. ومن ذلك نقترح تطوير طريقة تحسين مويجية متكيفة مع خصائص الصورة ودراسة مجاميع بيانات أوسع من المدروسة في البحث لغرض احداث تطوير أكبر في أداء التقنية.

الكلمات المفتاحية: التحويل المويجي المنفصل، التعبئة الصفرية، تحسين الدقة.

## 1. Introduction:

High-resolution images are essential in medical imaging (Greenspan, 2008), remote sensing (Demirel & Anbarjafari, 2010; Witwit et al., 2017), and astronomy industries (Al-Sadooni & van Loon, 2022; Hamza et al., 2020). Several approaches can be employed to enhance image resolution, including interpolation techniques, wavelets, and theourier transform (Agaian et al., 2001; Deeba et al., 2020). Wavelet methods have found applications in many crucial areas, including quantum field theory (QFT), harmonic analysis, and data compression, due to their ability to provide a localized analysis of a function and its multiresolution decomposition, which is utilized in decomposing Hilbert space (Bulut & Polyzou, 2013; Lee & Yamamoto, 1994).

Interpolation is a method for approximating a new pixel value based on the values of neighboring pixels in a low-resolution image Nevertheless, the computational (imgLR). complexity increases as the order of the interpolation factor increases. Standard interpolation methods involve nearest neighbour, bilinear, and bicubic (Patel & Mistree, 2013). Nearest neighbour interpolation uses the closest pixel for each new pixel, often resulting in blocky images. Bilinear averages the nearest 2×2 pixels for smoother images but can blur edges, while bicubic uses 4×4 pixels and cubic polynomials for sharper, more detailed results (Demirel & Anbarjafari, 2011; Karunakar et al., 2013).

Conventional interpolation methods rely on simple pixel averaging and do not consider the broader context of the image's structure. As a result, these methods often fail to preserve fine details and edges, which are crucial for maintaining image quality, especially in highresolution images. Additionally, these methods are limited in handling images with complex textures or noise, as they cannot distinguish between significant image features and noise.

Wavelet-based techniques emerged to overcome the limitations of traditional processing methods. They offer a multi-scale representation of an image, allowing for a more detailed analysis and manipulation of image features. Wavelet transforms (WT)-based methods enable the analysis of images at multiple resolutions by dividing them into different frequency ranges and scales (Azani Mustafa et al., 2019a). This lets the high-frequency ranges be enhanced in specific areas. Two of the basic wavelet transform-based techniques are the discrete wavelet transform (DWT) and wavelet zero-padding (WZP) (Yang et al., 2010a). DWT decomposes an image into multiple subbands, each containing different frequency components. The low-low (LL) subband contains most of the image's energy and general structure. Additionally, the low-high, high-low, and high-high subbands (LH et al.) are high-frequency components that encompass diagonal, horizontal, and vertical details, revealing and texture (Gonzalez & Woods. 2002; information Pimpalkhute et al., 2021).

functions Wavelet mathematical are functions used in the decomposition and reconstruction of images and signals, each with unique properties that make them suitable for various applications in image processing. The choice of wavelet function has a significant impact on the performance of the wavelet-based technique. This study examines the performance of the various wavelet functions (Lee & Yamamoto, 1994). Most wavelet functions have their wavelets; for example, Daubechies has wavelets that differ in the number of vanishing moments (N); this number determines the wavelet's ability to represent polynomial trends in data.

WZP fills the high-frequency subbands obtained from DWT with zeros to ensure smooth boundaries and decrease edge artifacts (Wu, 2019). The zero-padded subbands are combined with the interpolated LL subband using inverse DWT (IDWT) to reconstruct the high-resolution (HR) image. This technique is beneficial because it reduces discontinuities during the inverse transform and produces a sharper image. The performance of this technique varies depending on the interpolation method of the LL subband and the selection of the wavelet function. This approach investigates the effect of those two factors by applying different interpolation methods

and wavelet functions to standard, satellite, and astronomical images and comparing them in terms of PSNR and visual quality.

This work presents qualitative quantitative measurements for seven wavelet functions and their corresponding Descriptive statistics and tests were presented in the results subsection for reliable data analysis. All wavelets discussed in this study are suitable for Discrete Wavelet Transform (DWT) applications. Seven interpolation approaches were used to recreate the HR image of each quantitative supplementary measurement. A section is included. which presents а graphical representation of the Peak signal-to-noise ratio (PSNR) values for all the examined components. An appendix inserted in paper serves as a point of reference.

# 1.2. Literature survey

In 2007, Juang and Wu (Juang & Wu, 2007) utilized WZP for phase unwrapping in magnetic resonance imaging (MRI) brain phase images; such images suffer from phase discontinuities due to the wrapping of phase values, which leads to artificial phase jumps. WZP is used to smooth these discontinuities and improve image quality. DWT decomposes an image into four subbands, namely LL, LH, HL, and HH, and then zero-padding is applied to the highfrequency subbands. In contrast, conventional interpolation methods are applied to the LL subband. The high-resolution image is reconstructed by adding the LL interpolated image and the high-frequency subbands using IDWT. This approach demonstrates Daubechies wavelets combined with Lanczos interpolation yield the best PSNR and visual quality results. Juang's approach emphasizes the importance of selecting suitable wavelet functions and interpolation methods for achieving optimal image resolution enhancement using WZP.

Naidu et al. spectroradiometer (MODIS). The paper includes WZP, WZP with Cycle Spinning (WZP-CS), DWT, DWT combined with stationary wavelet transform (SWT), and error back Projection. The study evaluated MODIS images with a 250 m resolution in the Red and Near Infrared (NIR) spectral bands, comparing the superior enhancement of DWT-SWT with Error Back Projection in terms of PSNR. WZP is considered a basic wavelet technique. However, it yields a better PSNR compared to WZP-CS. Furthermore, this studv emphasizes importance of selecting suitable resolution

enhancement techniques to enhance the quality of satellite images.

To identify the key factors affecting the performance of wavelet-based image resolution enhancement, Witwit et al. (Witwit et al., 2016) proposed an optimal factor analysis (OFA) approach, in which they test essential factors such as the method to produce LR images, the choice of a wavelet function, the scale factor in resolution enhancement, and interpolation methods. Witwit's approach employs an algorithm to identify the optimal combination of all the studied factors. A key finding is that the choice of wavelet function influences the performance of WZP. However, not all current wavelet functions have been tested. Another result is that the technique used to produce LR images is crucial for obtaining higherresolution enhancement performance.

Traditional wavelet-based methods often use bicubic interpolations for high-frequency components, which can lead to noise. In contrast, Cui and Jinghong's approach utilizes a 2D wavelet transform to obtain low-frequency and threedirectional high-frequency subbands, then applies the DFT to the high-frequency subbands using the zero-padding technique. The original input image was enhanced by a confection and combined with the improved high-frequency subbands construct the HR image using an inverse 2D wavelet transform. This technique was tested on remote sensing images and demonstrated an improvement in resolution enhancement over traditional methods, as indicated by PSNR and RMSE.

Narmatha (Narmatha, 2020) studied the resolution enhancement of microarray images using a technique that is advantageous to the DWT, SWT, and WZP. The approach uses dwt to decompose the image into subbands in parallel, and SWT is applied to add high-frequency subbands of DWT and SWT together. Afterwards, a bicubic interpolation is applied to the input lowresolution image and the combined highfrequency subbands. The technique reduces artifacts using WZP and reconstructs the highfrequency image using IDWT. The performance of this technique is evaluated using PSNR, RMSE, entropy, and Contrast improvement Index (CII). It concludes that using DWT in conjunction with SWT provides superior resolution enhancement compared to using DWT alone.

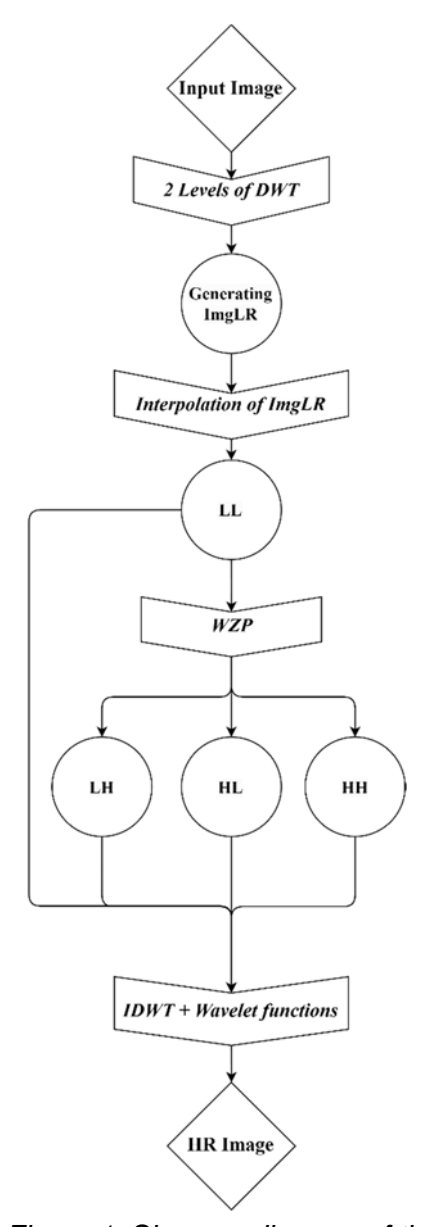


Figure 1. Shows a diagram of the proposed approach.

#### 2. MATERIALS AND METHODS:

The study encompasses multiple technical materials and delineates the methodology employed to gather the data for this investigation.

#### 2.1. Materials

In this study, the image enhancement technique was developed and implemented using MATLAB 2024a. The computational experiments were conducted on a workstation with an Intel Core i7 processor (7th Gen), 12GB of RAM, and Windows 10. The primary datasets used for testing and validating the enhancement technique are publicly available collections. The Lina dataset, with a size of 512×512, was acquired from (Repository, n.d.). Jupiter's ultraviolet image, with

a size of 1328×1285, was obtained from (Claire Andreoli, 2023). The Babylon University image, with a size of 3840×2160, was obtained from Google Earth at coordinates 99VX+RQ7, Hillah, Babylon Governorate.

Several MATLAB toolboxes were utilized, including the Image Processing Toolbox, Signal Processing Toolbox, and Computer Vision Toolbox. The experimental setup evaluated the technique's performance using the Peak signal-tonoise ratio (PSNR) metric. Specific wavelet functions and interpolation methods were selected based on their suitability for the DWT. Microsoft Excel program was used to collect and analyse the data.

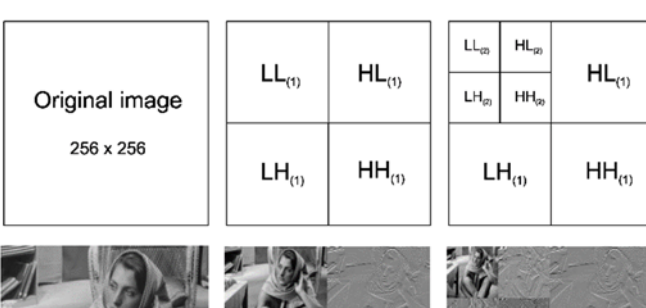
In a resolution enhancement study, a Python script was employed to create a heat map for visualizing the PSNR values obtained from applying 107 wavelet functions across eight interpolation methods. The script was designed to automatically identify and highlight the maximum PSNR value among all combinations, thus facilitating the identification of the most effective technique. The resulting heat map was then exported as a high-resolution PNG image, ensuring that the visual representation of the data is both detailed and suitable for academic analysis and publication. This automated approach not only enhances the efficiency of data analysis but also provides a clear and accurate depiction of the optimal wavelet and interpolation method combinations for each dataset.

# 2.2. Methodology

This study examines the effect of various wavelet functions and interpolation methods on Wavelet Zero Padding (WZP) performance for image resolution enhancement (D. Costa *et al.*, 2013). The loop program was written and run on MATLAB 2024a. **Figure 1** represents the methodology of the approach, which involves the following steps:

# 1. Image Decomposition Using DWT:

The high-resolution input image is decomposed using a two-level DWT to obtain subbands (LL, LH, HL, HH). **Figure 2** shows the process of decomposition using this method. The LL subband from the second level of decomposition is considered the low-resolution image (imgLR) that needs to be enhanced (Azani Mustafa *et al.*, 2019b).







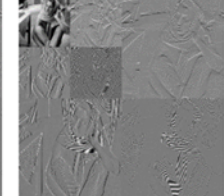


**Figure 2:** An example of image decomposition using two levels of DWT (D. G. Costa et al., 2013).

# 2. Interpolation of imgLR:

The imgLR is interpolated using different interpolation methods (nearest, bilinear, bicubic, triangle, Lanczos2, and Lanczos3) with a scale factor 2. The interpolated image (LLz) is obtained using the imresize () function (Kok & Tam, n.d.):

```
LLz = imresize (imgLR,
2,'interpolation_method');
```

# 3. Wavelet Zero Padding (WZP):

High-frequency subbands (LHz, HLz, HHz) are initialized to zero matrices of the same size as LLz.

```
LHz = zeros(size(LLz));
HLz = zeros(size(LLz));
HHz = zeros(size(LLz));
```

## 4. Image Reconstruction Using IDWT:

The LLz, LHz, HLz, and HHz subbands are combined using the Inverse Discrete Wavelet Transform (IDWT) to reconstruct the high-resolution image (imgHR).

```
imgHR = idwt2(LLz, LHz, HLz, HHz,
'WaveletFunction');
```

Various wavelet functions can be used to reconstruct the high-resolution image.

# 5. Evaluation of Wavelet Functions and Interpolation Methods:

A loop iterates through different wavelet functions (e.g., Haar, Daubechies, Biorthogonal) and their filters, and the interpolation methods (nearest, bilinear, bicubic, Lanczos). For each combination, the peak signal-to-noise ratio (PSNR) is calculated to assess the quality of the reconstructed high-resolution image. This study aims to determine the optimal combinations for

maximizing image resolution enhancement using WZP by varying the wavelet functions and interpolation methods.

## 3. RESULTS AND DISCUSSION:

#### 3.1. Results

The study evaluates the performance of different wavelet functions combined with various interpolation methods in terms of PSNR. It utilizes a program that iterates over all the wavelet functions applicable to DWT and seven interpolation methods, which are designed and applied to three data sets.

PSNR is used to measure the maximum error magnitude between the original and processed imagery, thereby providing a metric of the qualitative enhancement achieved. The PSNR is computed using Equation 1 (Gonzalez & Woods, 2002):

$$PSNR = 10 \log_{10} \left( \frac{R^2}{MSE} \right)$$
 (Eq. 1)

Where R is the maximum fluctuation in the input image data, and MSE denotes the mean squared error between the provided input image.  $I_{in}$  and the original image  $I_{org}$ , Calculated with Equation 2 (Anbarjafari & Demirel, 2010):

$$MSE = \frac{\sum_{i,j} \left( I_{in}(i,j) - I_{org}(i,j) \right)^2}{M \times N}$$
 (Eq. 2)

Where M and N represent the sizes of the two images, the evaluation includes images of Lina, Jupiter in ultraviolet, and Babylon University's College of Science. These images represent standard, astronomical, and remote sensing images. The program generates an Excel sheet containing the PSNR values for eight interpolation methods and 107 wavelet functions. It also provides a figure displaying the visual results for each family and their corresponding filters. Appendix A includes a heat map of all the PSNR results for Lina's image.

**Tables 1** to **9** present the statistical analysis of the datasets under study, which includes interpolation methods and wavelet functions. **Tables 1** to **6** present the best PSNR performance and descriptive statistics for each dataset.

Advanced interpolation methods, such as bicubic, Lanczos3, and cubic, yielded higher PSNR for standard photos. The results of the Lina dataset showed that the coif2 wavelet gave the

highest PSNR values across all the interpolation methods. They range from 25.121 for the nearest box to 26.840 for lanczos3, the highest PSNR value. Meanwhile, the fk8 wavelet achieves the highest PSNR for all the interpolation methods for the Jupiter dataset. However, bilinear and triangle methods achieve a top PSNR of 32.208 when combined with the fk8 wavelet. The best PSNR values were achieved for the satellite image by applying various Bior wavelets. However, bilinear and triangle interpolation methods return a slightly higher PSNR than other interpolation methods. These findings are evident in **Tables 1** to **3**.

Tables 4 to 6 represent the descriptive statistics of interpolation methods for all datasets. The range of PSNR values in the three tables is roughly the same, from approximately 12.47 to 13.68 for the Lina dataset, from 10.5 to 10.94 for the Jupiter dataset, and from 1.04 to 1.06 for the Babylon dataset. This suggests that interpolation methods result in a comparable spectrum. Furthermore, on average, different interpolation methods yield similar PSNR values for the three datasets; this can be concluded from the relatively close PSNR mean of the other interpolation methods, ranging from 19.9 to 20.5 for the Lina dataset, from 28.85 to 29.2 for the Jupiter dataset, and from 11.33 to 11.40 for the Babylon dataset. All interpolation methods have the same variability level, deduced from the close values of standard deviations and variance. Negative close to zero skewness values indicate that the PSNR distribution for all interpolation methods is slightly left-skewed, but the skewness is not extreme. In addition, the kurtosis values are all negative, indicating that the PSNR distribution is thinner at its tails and has a flatter peak than the normal distribution. The small kurtosis values suggest that the distribution is not far from normal. The reliability of the sample means and other statistics is obtained due to the relatively small standard errors of mean, skewness, and kurtosis.

The significance values of data are zero along all interpolation methods, according to the Shapiro-Wilk test of normality, as shown in **Table 7**. A zero value of significance indicates that the data is normally distributed. To evaluate the differences in PSNR values across various interpolation methods, we first tested the assumption of homogeneity of variances using Levene's test (Glass, 1966; Loh, 1987). The results indicated no significant differences in variances across the groups (Levene's test, p > 0.05 for all tests), confirming that the assumption of homogeneity of variances was met. The non-parametric Kruskal-Wallis Test gave a significant

value of 0.482 for all interpolation methods, which is greater than alpha (0.05), so the null hypothesis is retained for each interpolation method.

ANOVA statistical test **PSNR** performance is represented in Tables 8 and 9. This test compares means across multiple groups determine any statistically significant differences. The variation is tested between groups and within each group(Lars & Wold, 1989). The sum of squares (SS), Degrees of freedom (Df), Mean square (MS), the ratio between MS between groups to the MS within groups (F-value), the probability of significant differences (P-value), and F critical (F crit) are shown. Table 8 shows that the F-value (0.422, 0.176, 0.732) is less than F crit (2.0204, 2.204, 2.0204), and the p-value (0.888, 0.990, 0.644) is greater than 0.05 for Lina image, Jupiter, and Babylon datasets, respectively. These findings suggest that the choice of interpolation method does not significantly affect the PSNR values. On the other hand, in Table 9, the ANOVA results for PSNR performance, where wavelet functions rather than interpolation methods group data, indicate that there is a significant variation between the wavelet functions; the between-group sum of squares (SS) is much larger than the within-group SS for all datasets. A substantial between-group variance is also observed; the mean square (MS) between groups is larger than the MS within groups. The P-values for all data sets are zero, less than the significance level of 0.05, and the F-values are greater than the critical F-value (F-cret.). Suggests that the differences between the wavelet functions are statistically significant.

Figure 3 illustrates a lower performance of high-order Daubechies wavelets, but a higher PSNR for other wavelets, across the three datasets. The overall PSNR value of the Jupiter image was the highest among the three datasets; this image has fewer details than the other two. The WZP enhancement of the Babylon dataset yielded the lowest PSNR value across all wavelet functions.

The Q-Q plots in **Figure 4** indicate that the data points from all interpolation methods follow a roughly straight line, suggesting that the PSNR values are approximately normally distributed. While some minor deviations were observed at the tails, these were not severe, indicating that the normality assumption is reasonably satisfied. **Figure 4** shows the visual representation of WZP. The fk8 wavelet, combined with the bilinear interpolation method, produced a smoother image and greater clarity than db7 and db45, both of

which used the box interpolation method. The normality of the PSNR values for each interpolation method was assessed using Q-Q plots.

#### 3.2. Discussion

Applying homogeneity of variances, normality tests, and Analysis of Variance (ANOVA) is crucial when evaluating performance of resolution enhancement techniques, particularly when comparing different interpolation methods and wavelet functions based on PSNR values. Ensuring homogeneity of variances means that the data in each group have similar levels of variation, which is necessary for ANOVA to give accurate results. Performing normality checks to ensure that the data in each group follows a normal distribution, which is a prerequisite for conducting reliable statistical tests. ANOVA then helps to compare the average PSNR values across different methods to see if there are significant differences. Together, these methods ensure that the analysis of which technique works best is both sound and dependable.

The selection of wavelet functions is impactful significantly more than interpolation methods. The results reveal substantial variations in PSNR values among different wavelet functions, while no significant differences have been observed among the interpolation methods. Statistical analysis confirms that there is no statistically significant difference in the distributions of PSNR values across the interpolation methods; thus, the null hypothesis for each method across all wavelet functions is retained, as supported by the ANOVA tests.

Each wavelet function has its own set of advantages and limitations. Coiflets demonstrate compact support, which means they possess a limited number of non-zero coefficients. This characteristic allows coif2 to preserve edges and details while minimizing artifacts. Additionally, Coiflets are nearly symmetric and orthogonal, with symmetry aiding in reducing phase distortions and orthogonality, ensuring wavelet energy preservation.

Coiflets vary in terms of vanishing moments and filter length, which affects their computational complexity. As the value of N increases in CoifN (i.e., Coif1, Coif2, Coif3 to CoifN), the number of vanishing moments and the length of the filter also increase. The selection of a Coiflet must balance these two characteristics; using higher-order Coiflets leads to a smoother

signal representation(Dong Wei *et al.*, n.d.; Wei, 1998).

Astronomical images often contain large areas with smooth gradients, such as gaseous regions of planets. The fk8 wavelet is better suited for representing these smooth regions because it has many vanishing moments. Additionally, the fk8 wavelet can accurately capture different frequency components of the image due to its fine frequency localization properties.

Biorthogonal (Bior) wavelets possess multiple vanishing moments in wavelet and scaling functions. This characteristic enables the wavelet to capture polynomial trends and smooth variations effectively (e.g., water, agricultural fields) in the data while preserving the geometric structures of Earth images, such as buildings and roads. The Bior wavelet (3.1, 3.3, 3.5, 3.7, 3.9) offers a well-balanced trade-off between signal representation accuracy and computational complexity (ang *et al.*, 2010b).

The varying performance of wavelet functions in high-resolution image reconstruction is attributed to the distinct mathematical properties of each wavelet and the specific characteristics of the images being processed. Wavelets like Coif2, with its balanced time and frequency localization, excel in enhancing images with smooth regions and well-defined edges, such as the Lena image. In contrast, the Bior family, known for its effective localization, is better suited for complex textures found in satellite images. The FK8 wavelet outperforms others in processing astronomical images, such as those of Jupiter, where it effectively captures the unique spatial frequency distribution.

#### 4. CONCLUSION:

WZP is an essential technique for resolution enhancement. It reduces edge artifacts by smoothing the image while preserving image features. The performance of this technique depends on selecting a suitable wavelet function for the studied dataset and requires a proper interpolation method.

Additionally, each wavelet function has unique properties and performs better on some datasets than others. This can be indicated by the superiority of coif2 for the Lina dataset, while fk8 excelled in the Jupiter dataset. However, Bior was more effective for remote sensing data sets. Coif2 has higher vanishing moments and can better capture and preserve fine details and edges; its

near-symmetry characteristic helps reconstruct edges without artifacts. This is also the case for fk8; both wavelet functions exhibit time-frequency localization, ensuring that both low-frequency components are effectively represented.

To further enhance performance, we recommend developing adaptive wavelet techniques that dynamically adjust the wavelet function based on the specific characteristics of the input image. These adaptive techniques should account for critical image features such as edges, textures, and other relevant aspects. By modifying the wavelet function to better align with these characteristics, the technique can provide more precise and effective image processing.

Looking ahead, future research should explore the impact of different wavelet functions on broader array of datasets and consider alternative resolution enhancement techniques beyond WZP. Expanding the scope of the investigation to include a wider range of datasets will provide users of WZP with clear insights into which wavelet function best suits their specific needs. Additionally, the study should not be limited to WZP; it is also crucial to evaluate other waveletbased image enhancement techniques. Techniques utilizing Discrete Wavelet Transform (DWT), Continuous Wavelet Transform (CWT), and other wavelet applications in image reconstruction should also be examined. By comparing the effectiveness of various wavelet functions across multiple enhancement techniques, we can deepen our understanding of their utility and performance, thereby advancing the field of resolution enhancement and offering more versatile solutions to meet diverse imaging requirements.

# 5. Appendix: PSNR Heatmap

This heat map of data for the Lina image was provided to reference the PSNR of WZP for each wavelet function and the correspondence interpolation method.

# 6. DECLARATIONS

# 6.1. Study Limitations

This study acknowledges several limitations: Limited Datasets: The research was conducted using a limited number of datasets, specifically the Lina, Jupiter, and Babylon datasets. This constraint may affect the generalizability of the findings to other types of images or datasets.

The study did not include a comparative analysis with other state-of-the-art image resolution enhancement methods. Future work should incorporate such comparisons to contextualize the performance of the proposed methods against the current leading techniques in the field.

#### 6.2. Acknowledgment

The authors would like to express their gratitude to the following institutions and organizations:

- University of Babylon, College of Science, Department of Physics, for providing the necessary support and facilities to conduct this research.
- NASA: To grant access to astronomical images used in this study.
- Google Earth for providing access to remote sensing images integral to the research.

# 6.3. Funding

The Corresponding Author funded the research presented in this paper. No external funding sources were utilized in the preparation of this work. In accordance with the ethical guidelines of the Periódico Tchê Química, which do not allow donations from authors with manuscripts under evaluation (even when research funds are available), or in cases of authors' financial constraints, publication costs were fully absorbed by the journal under our Platinum Open Access policy, through the support of the Araucária Scientific Association (https://acaria.org/). This policy aims to ensure complete independence between the editorial process and any financial aspects, reinforcing our commitment to scientific integrity and equity in knowledge dissemination.

## 6.4. Competing Interests

The authors declare that they have no competing interests.

#### 6.5. Open Access Declaration

This article is distributed under the Creative Commons Attribution License terms, which permits unrestricted use, distribution, and reproduction in any medium, provided the original author and source are credited. By making this

research openly accessible, we aim to promote the dissemination of knowledge and facilitate the advancement of science by allowing researchers, practitioners, and the public to access and utilize our findings freely.

#### 7. REFERENCES:

- Agaian, S. S., Panetta, K., & Grigoryan, A. M. (2001). Transform-based image enhancement algorithms with performance measure. *IEEE Transactions on Image Processing*, 10(3), 367–382. https://doi.org/10.1109/83.908502
- Al-Sadooni, A. Ab., & van Loon, J. Th. (2022). The kinematics and physical properties for some H II regions to the northeast of NGC 4945\*\*. 080049. https://doi.org/10.1063/5.0067075
- Anbarjafari, G., & Demirel, H. (2010). Image Super Resolution Based on Interpolation of Wavelet Domain High Frequency Subbands and the Spatial Domain Input Image. *ETRI Journal*, 32(3), 390–394. https://doi.org/10.4218/etrij.10.0109.0303
- Azani Mustafa, W., Yazid, H., Khairunizam, W., Aminuddin Jamlos, M., Zunaidi, I., Razlan, Z. M., & Shahriman, A. B. (2019a). Image Enhancement Based on Discrete Cosine Transforms (DCT) and Discrete Wavelet Transform (DWT): A Review. *IOP Conference Series: Materials Science and Engineering*, 557(1), 012027. https://doi.org/10.1088/1757-899X/557/1/012027
- Azani Mustafa, W., Yazid, H., Khairunizam, W., Aminuddin Jamlos, M., Zunaidi, I., Razlan, Z. M., & Shahriman, A. B. (2019b). Image Enhancement Based on Discrete Cosine Transforms (DCT) and Discrete Wavelet Transform (DWT): A Review. *IOP Conference Series: Materials Science and Engineering*, 557(1), 012027. https://doi.org/10.1088/1757-899X/557/1/012027
- Bulut, F., & Polyzou, W. N. (2013). Wavelets in field theory. *Physical Review D*, 87(11), 116011. https://doi.org/10.1103/PhysRevD.87.1160 11
- Claire Andreoli. (2023, November 3).
   Hubble Provides Unique Ultraviolet View of Jupiter. NASA, ESA, and M. Wong (University of California Berkeley); Processing: Gladys Kober (NASA/Catholic University of America).
- 8. Costa, D. G., Affonso Guedes, L., Vasques,

- F., & Portugal, P. (2013). Energy-efficient packet relaying in wireless image sensor networks exploiting the sensing relevancies of source nodes and DWT coding. *Journal of Sensor and Actuator Networks*, 2(3), 424–448.
- https://doi.org/10.3390/jsan2030424
- Costa, D., Guedes, L., Vasques, F., & Portugal, P. (2013). Energy-Efficient Packet Relaying in Wireless Image Sensor Networks Exploiting the Sensing Relevancies of Source Nodes and DWT Coding. *Journal of Sensor and Actuator Networks*, 2(3), 424–448. https://doi.org/10.3390/jsan2030424
- Deeba, F., Kun, S., Ali Dharejo, F., & Zhou, Y. (2020). Wavelet-Based Enhanced Medical Image Super Resolution. *IEEE Access*, 8, 37035–37044. https://doi.org/10.1109/ACCESS.2020.297 4278
- 11. Demirel, H., & Anbarjafari, G. (2010). Satellite Image Resolution Enhancement Using Complex Wavelet Transform. *IEEE Geoscience and Remote Sensing Letters*, 7(1), 123–126. https://doi.org/10.1109/LGRS.2009.202844
- 12. Demirel, H., & Anbarjafari, G. (2011). Discrete Wavelet Transform-Based Satellite Image Resolution Enhancement. *IEEE Transactions on Geoscience and Remote Sensing*, 49(6), 1997–2004. https://doi.org/10.1109/TGRS.2010.210040
- Dong Wei, Bovik, A. C., & Evans, B. L. (n.d.). Generalized coiflets: a new family of orthonormal wavelets. Conference Record of the Thirty-First Asilomar Conference on Signals, Systems and Computers (Cat. No.97CB36136), 1259–1263. https://doi.org/10.1109/ACSSC.1997.6791 06
- 14. Glass, G. V. (1966). Testing Homogeneity of Variances. Http://Dx.Doi.Org/10.3102/0002831200300 3187, 3(3), 187–190. https://doi.org/10.3102/0002831200300318 7
- 15. Gonzalez, R. C., & Woods, R. E. (2002). *Digital Image Processing* (2nd ed.). Prentice Hall.
- 16. Greenspan, H. (2008). Super-Resolution in Medical Imaging. *The Computer Journal*, 52(1), 43–63. https://doi.org/10.1093/comjnl/bxm075
- 17. Hamza, H. A., Sadooni, A. Ab. Al, & Loon,

- J. Th. van. (2020). Feedback from Ionized Outflows Traced Across the Nearly Edge-on Disk of the Nearby Seyfert 2 Galaxy NGC 4945\*. *NeuroQuantology*, 18(12), 06–17. https://doi.org/10.14704/nq.2020.18.12.NQ 20232
- Juang, P.-A., & Wu, M.-N. (2007). MRI Brain Phase Image Unwrapping Process by Wavelet Zero-Padding Technique. Third International Conference on Intelligent Information Hiding and Multimedia Signal Processing (IIH-MSP 2007), 229–232. https://doi.org/10.1109/IIH-MSP.2007.224
- 19. Karunakar, P., Praveen, V., & Kumar, O. R. (2013). Discrete wavelet transform-based satellite image resolution enhancement. *Advance in Electronic and Electric Engineering*, 3(4), 405–412.
- 20. Kok, C.-W., & Tam, W.-S. (n.d.). Digital image interpolation in MATLAB. 336. Retrieved July 3, 2024, from https://www.wiley.com/en-cn/Digital+Image+Interpolation+in+Matlab-p-9781119119647
- 21. Lars, S., & Wold, S. (1989). Analysis of variance (ANOVA). *Chemometrics and Intelligent Laboratory Systems*, *6*(4), 259–272. https://doi.org/10.1016/0169-7439(89)80095-4
- 22. Lee, D. T. L., & Yamamoto, A. (1994). Wavelet analysis: theory and applications. *Hewlett-Packard Journal*, *45*(6).
- 23. Loh, W. Y. (1987). Some modifications of levene's test of variance homogeneity. Journal of Statistical Computation and Simulation, 28(3), 213–226. https://doi.org/10.1080/0094965870881103 0
- 24. Naidu, S. V., Garg, A., Yahia, H., & Singh, D. (2015). A comparison of wavelet based techniques for resolution enhancement of Moderate Resolution satellite images. 2015 National Conference on Recent Advances in Electronics & Computer Engineering (RAECE), 263–266. https://doi.org/10.1109/RAECE.2015.7510 203
- 25. Narmatha, D. (2020). Resolution Enhancement of Microarray Image Using DWT AND SWT. *Journal of Analog and Digital Devices*, *5*(3), 20–28.
- Patel, V., & Mistree, K. (2013). A review on different image interpolation techniques for image enhancement. *International Journal* of *Emerging Technology and Advanced Engineering*, 3(12), 129–133.
- 27. Pimpalkhute, V. A., Page, R., Kothari, A.,

- Bhurchandi, K. M., & Kamble, V. M. (2021). Digital Image Noise Estimation Using DWT Coefficients. *IEEE Transactions on Image Processing*, 30, 1962–1972. https://doi.org/10.1109/TIP.2021.3049961
- 28. Repository. (n.d.). Retrieved July 6, 2024, from https://links.uwaterloo.ca/Repository.html
- 29. Shapiro, S. S., Wilk, M. B., & Chen, H. J. (1968). A Comparative Study of Various Tests for Normality. *Journal of the American Statistical Association*, 63(324), 1343–1372. https://doi.org/10.1080/01621459.1968.104 80932
- 30. Wei, D. (1998). Coiflet-type wavelets: theory, design, and applications. The University of Texas at Austin.
- 31. Witwit, W., Zhao, Y., Jenkins, K., & Zhao, Y. (2016). An Optimal Factor Analysis Approach to Improve the Wavelet-based Image Resolution Enhancement Techniques.

- 32. Witwit, W., Zhao, Y., Jenkins, K., & Zhao, Y. (2017).Satellite image resolution enhancement using discrete wavelet transform and new edge-directed interpolation. Journal of Electronic Imaging, 023014. https://doi.org/10.1117/1.JEI.26.2.023014
- Wu, M. Te. (2019). Wavelet transform based on Meyer algorithm for image edge and blocking artifact reduction. *Information Sciences*, 474, 125–135. https://doi.org/10.1016/J.INS.2018.09.058
- 34. Yang, Y., Su, Z., & Sun, L. (2010a). Medical image enhancement algorithm based on wavelet transform. *Electronics Letters*, *46*(2), 120–121.
- 35. Yang, Y., Su, Z., & Sun, L. (2010b). Medical image enhancement algorithm based on wavelet transform. *Electronics Letters*, 46(2), 120. https://doi.org/10.1049/el.2010.2063

**Table 1.** The best performance of wavelet functions in terms of PSNR for different interpolation methods and their corresponding wavelet functions, each method applied to a Lina image. The values in bold indicate the maximum PSN.

Interpolation Method	Max-PSNR	Wavelet
nearest	25.121	coif2
bilinear	25.561	coif2
bicubic	26.525	coif2
box	25.121	coif2
triangle	25.561	coif2
cubic	26.525	coif2
lanczos2	26.559	coif2
lanczos3	26.840	coif2

**Table 2.** The best performance of wavelet functions in terms of PSNR for different interpolation methods, each method applied to the astronomical image. The values in bold indicate maximum PSNRs.

Interpolation Method	Max-PSNR	Wavelet
nearest	31.702	fk8
bilinear	32.208	fk8
bicubic	31.904	fk8
box	31.702	fk8
triangle	32.208	fk8
cubic	31.904	fk8
lanczos2	31.896	fk8
lanczos3	31.799	fk8

**Table 3.** The best performance of wavelet functions in terms of PSNR for different interpolation methods, each method applied to the satellite image. The values in bold indicate maximum PSNRs.

Interpolation Method	Highest PSNR	Wavelet
nearest	11.648	Bior(3.1,3.3,3.5,3.7,3.9)
bilinear	11.700	Bior(3.1,3.3,3.5,3.7,3.9)
bicubic	11.639	Bior(3.1,3.3,3.5,3.7,3.9)
box	11.648	Bior(3.1,3.3,3.5,3.7,3.9)
triangle	11.700	Bior(3.1,3.3,3.5,3.7,3.9)
cubic	11.639	Bior(3.1,3.3,3.5,3.7,3.9)
lanczos2	11.639	Bior(3.1,3.3,3.5,3.7,3.9)
lanczos3	11.628	Bior(3.1,3.3,3.5,3.7,3.9)

**Table 4.** Descriptive Statistics of interpolation methods for the Lina Dataset. Bold values are the maximum value in a row.

					nterpola	tion Meth	od		
		nearest	bilinear	bicubic	box	triangle	cubic	lanczos2	lanczos3
	N	106	106	106	106	106	106	106	106
	Range	12.467	12.660	13.435	12.467	12.660	13.435	13.461	13.682
<u>၁</u>	Mean	19.891	20.522	20.510	19.891	20.522	20.510	20.510	20.487
Statistic	Std. Deviation	4.292	4.494	4.674	4.292	4.494	4.674	4.679	4.725
Ś	Variance	18.424	20.196	21.850	18.424	20.196	21.850	21.891	22.325
	Skewness	-0.496	-0.574	-0.508	-0.496	-0.574	-0.508	-0.506	-0.482
	Kurtosis	-1.409	-1.396	-1.439	-1.409	-1.396	-1.439	-1.440	-1.452
Error	Mean	0.417	0.436	0.454	0.417	0.436	0.454	0.454	0.459
_	Skewness	0.235	0.235	0.235	0.235	0.235	0.235	0.235	0.235
Std	Kurtosis	0.465	0.465	0.465	0.465	0.465	0.465	0.465	0.465

**Table 5.** Descriptive Statistics of various interpolation methods for the Jupiter Dataset. Bold values are the maximum value in a row.

					nterpola	tion Meth	od		
		nearest	bilinear	bicubic	box	triangle	cubic	lanczos2	lanczos3
	N	106	106	106	106	106	106	106	106
	Range	10.507	10.942	10.694	10.507	10.942	10.694	10.687	10.603
<u>:</u>	Mean	28.858	29.237	29.019	28.858	29.237	29.019	29.015	28.950
Statistic	Std. Deviation	3.527	3.693	3.611	3.527	3.693	3.611	3.610	3.582
Ś	Variance	12.438	13.637	13.040	12.438	13.637	13.040	13.029	12.834
	Skewness	-1.049	-1.045	-1.045	-1.049	-1.045	-1.045	-1.045	-1.046
	Kurtosis	-0.568	-0.591	-0.590	-0.568	-0.591	-0.590	-0.590	-0.588
or.	Mean	0.343	0.359	0.351	0.343	0.359	0.351	0.351	0.348
I. Error	Skewness	0.235	0.235	0.235	0.235	0.235	0.235	0.235	0.235
Std	Kurtosis	0.465	0.465	0.465	0.465	0.465	0.465	0.465	0.465

**Table 6.** Descriptive Statistics of various interpolation methods for the Babylon Dataset. Bold values are the maximum value in a row.

			Interpolation Method						
		nearest	bilinear	bicubic	box	triangle	cubic	lanczos2	lanczos3
	N	106	106	106	106	106	106	106	106
	Range	1.063	1.043	1.047	1.063	1.043	1.047	1.047	1.047
<u>၁</u>	Mean	11.332	11.406	11.344	11.332	11.406	11.344	11.344	11.332
Statistic	Std. Deviation	0.383	0.386	0.386	0.383	0.386	0.386	0.386	0.385
Ś	Variance	0.147	0.149	0.149	0.147	0.149	0.149	0.149	0.148
	Skewness	-1.062	-1.064	-1.072	-1.062	-1.064	-1.072	-1.072	-1.073
	Kurtosis	-0.589	-0.602	-0.586	-0.589	-0.602	-0.586	-0.585	-0.582
or	Mean	0.037	0.038	0.037	0.037	0.038	0.037	0.037	0.037
I. Error	Skewness	0.235	0.235	0.235	0.235	0.235	0.235	0.235	0.235
Std.	Kurtosis	0.465	0.465	0.465	0.465	0.465	0.465	0.465	0.465

**Table 7.** Shapiro-Wilk Test of normality (Shapiro et al., 1968) for the PSNR outcomes of interpolation methods along wavelet functions.

		Lina		Jupite	er	Babylon	
		Statistic	Sig.	Statistic	Sig.	Statistic	Sig.
	nearest	.851	.000	.734	.000	.734	.000
u	bilinear	.816	.000	.726	.000	.726	.000
tion Is	bicubic	.836	.000	.726	.000	.726	.000
terpolatio Methods	box	.851	.000	.734	.000	.734	.000
rpc eth	triangle	.816	.000	.726	.000	.726	.000
Inte	cubic	.836	.000	.726	.000	.726	.000
=	lanczos2	.836	.000	.726	.000	.726	.000
	lanczos3	.842	.000	.726	.000	.726	.000

**Table 8:** ANOVA statistical test for interpolation method groups, where the effect size is 1, and the confidence interval is 95%. The results suggest that there are no significant differences between interpolation methods.

		Li	na	Jup	iter	Babylon		
		Between Groups	Within Groups	Between Groups	Within Groups	Between Groups	Within Groups	
of Variation	SS	60.984391	17341.47	16.04748	10929.74	0.76039	124.6111	
aria	Df	7	840	7	840	7	840	
of V	MS	8.7120558	20.64461	2.292497	13.0116	0.108627	0.148347	
_	F	0.4220014		0.176189		0.732253		
Source	P-value	0.8888972		0.990072		0.644666		
S	F crit	2.0204628		2.020463		2.020463		

**Table 9:** ANOVA statistics of PSNR performance at significance level 0.05. where the effect size is one, and the confidence interval is 95%. Wavelet functions grouped the data; results suggest that there is a significant difference across wavelet functions.

		Lin	a	Jupi	ter	Babylon		
		Between Groups	Within Groups	Between Groups	Within Groups	Between Groups	Within Groups	
ion	SS	17287.632	114.826	10924.328	21.461	124.566	0.805	
of Variation	Df	105.000	742.000	105.000	742.000	105.000	742.000	
f Va	MS	164.644	0.155	104.041	0.029	1.186	0.001	
	F	1063.920		3597.161		1092.908		
Source	P- value	0.000		0.000		0.000	-	
	F crit	1.259		1.259		1.259321834		

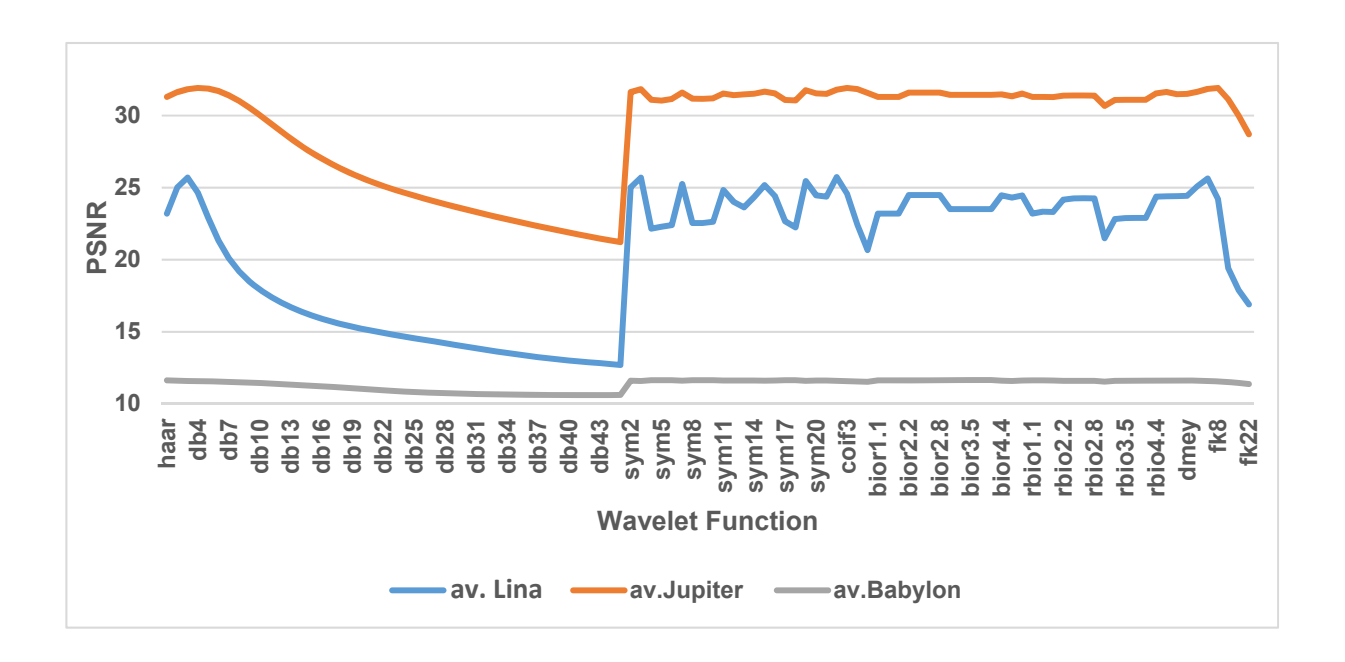


**Figure 3.** PSNR performance of wavelet functions for the Lina, Jupiter, and Babylon datasets, where each point represents the average of the eighth interpolation method. A clear difference appears in the results; Daubechies wavelets yield the lowest PSNR, while Coiflet and fk8 have very close results.

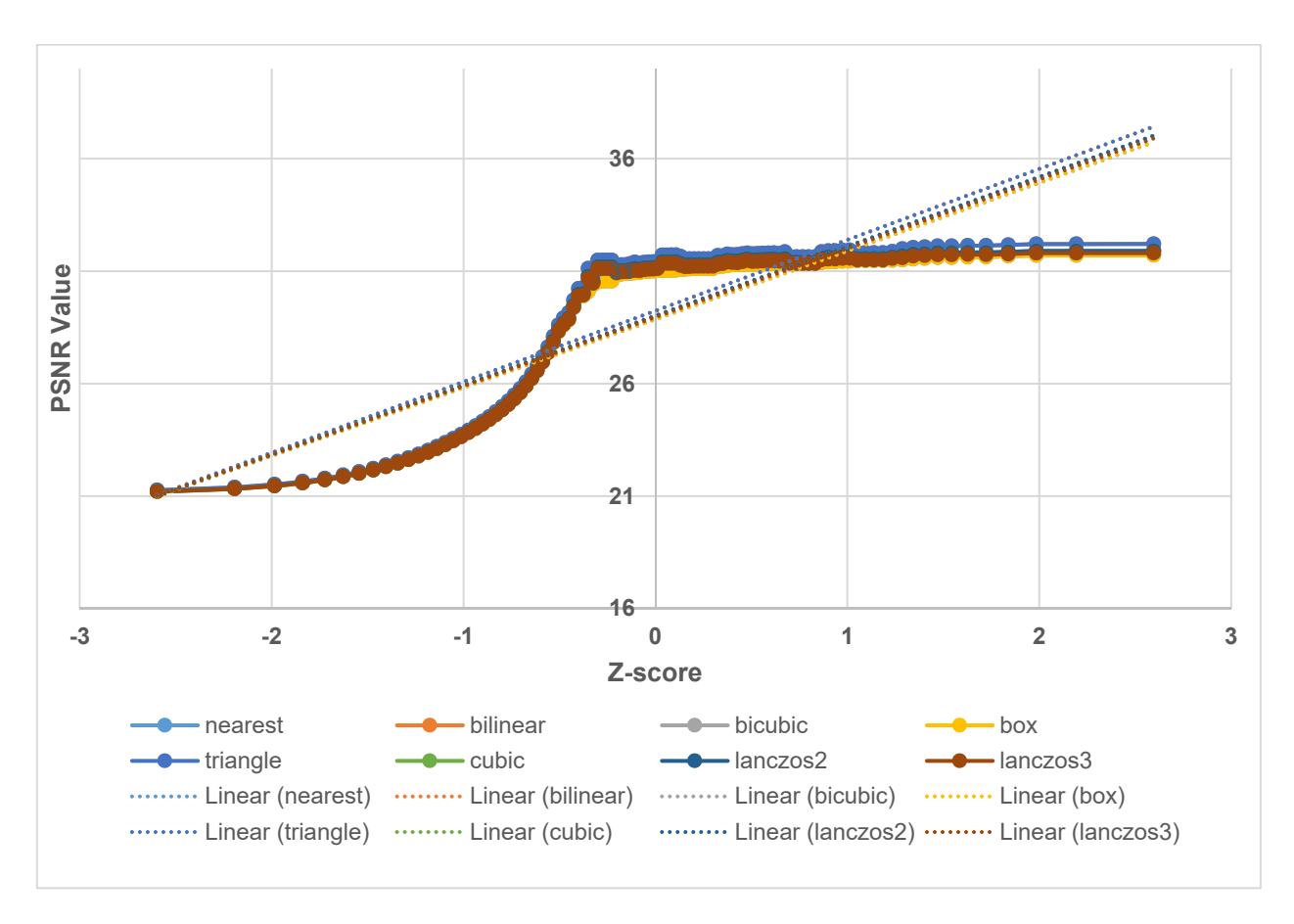


**Figure 4.** The Jupiter PSNR results' Q-Q plot shows roughly linear behavior for all groups with a slight skew in the tails.

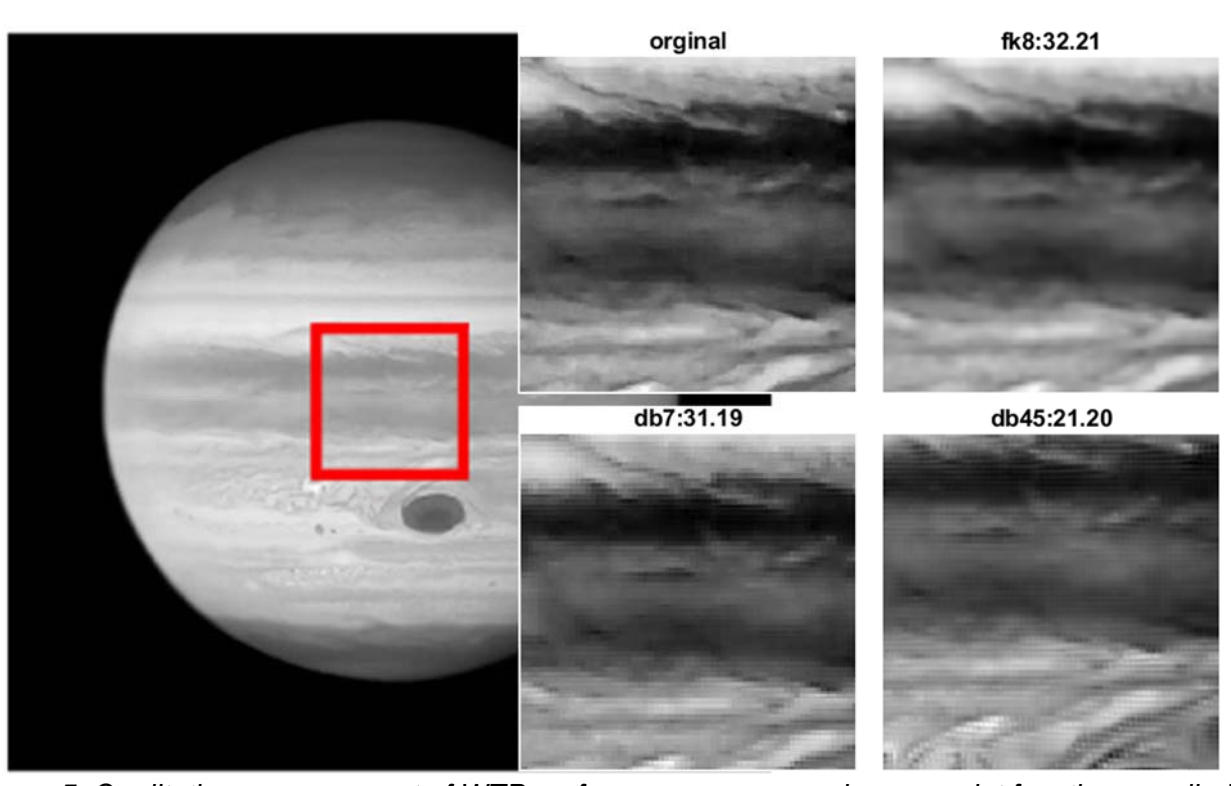


**Figure 5.** Qualitative measurement of WZP performance across various wavelet functions applied to Jupiter in the ultraviolet image. The red rectangle indicates the cropped portion of the original image; the maximum PSNR achieved using fk8 and the bilinear interpolation method is shown in the upper right image. The median PSNR is at the lower left result from the db7, and the minimum PSNR is at the lower correct result from the db45 and box interpolation method

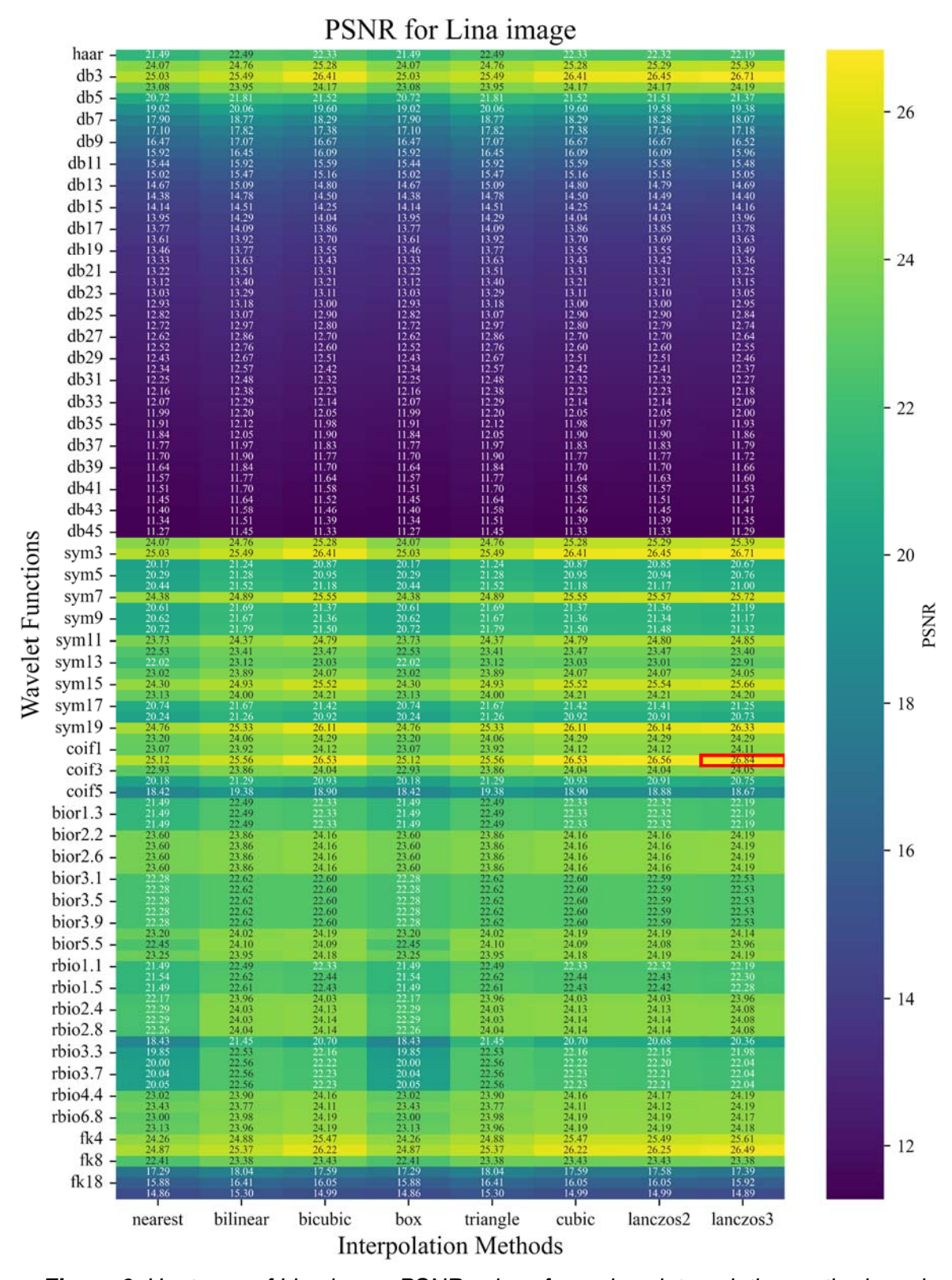


**Figure 6.** Heat map of Lina image PSNR values for various interpolation methods and wavelet functions; the red rectangle marks the maximum PSNR value.